Improved structure-switch aptamer based fluorescent Pb^{2+} biosensor utilizing binding induced quenching of AMT to G-quadruplex

Fenghua Geng, [a,b,#] Dandan Wang[c,#], Li Feng[a,*] Guixin Li[c], Maotian Xu[b,*]

[a]*National Engineering Research Center of Coal Preparation and Purification; Key Laboratory of Coal Processing and Effcient Utilization of Ministry of Education, School of Chemical Engineering and Technology, China University of Mining & Technology, Xuzhou 221116, China*

[b]*Henan Key Laboratory of Biomolecular Recognition and Sensing, College of Chemistry and Chemical Engineering, Henan Joint International Research Laboratory of Chemo/Biosensing and Early Diagnosis of Major Diseases, Shangqiu Normal University, Shangqiu, 476000, China*

[c]*College of Chemistry and Chemical Engineering, Xinjiang Normal University, Urumqi, 830054, China*

[#] *The co-first author.*

* Corresponding authors. *E-mail addresses:*8422127@alu.fudan.edu.cn (L. Feng), xumaotian@sqnu.edu.cn (M. T. Xu)

1. Materials and methods

1.1 Materials and apparatus

4'-aminomethyltrioxsalen hydrochloride (AMT) and tris(hydroxymethyl)aminomethane (Tris) were available from Sigma-adlrich company (St. Louis, USA); 2-morpholinoethanesulfonic acid (MES) was purchased from Serva (Shanghai, China); $Pb(NO_3)_2$ and other salts are A. R. grade from Sinopharm Chemical Reagent Co., Ltd. (Shanghai, China). The solutions were prepared using deionized water (18.2 MΩ.cm) which was produced from Milli-Q Advantage A10 (Molsheim, France). The pH was measured using a Leici pHS-3C acidity meter (Shanghai, China). All DNA (Table S1) sequences were bought from Shanghai Sangon Co., Ltd. (Shanghai, China). Inductively coupled plasma-atomic emission spectrometry (ICP-AES) (PerkinElmer Optima 8000, USA) was used to detect Pb^{2+} in 1% human serum.

1.2 Fluorescence measurements

The emission spectra were monitored by a Hitachi F-7000 fluorescence spectrometer. For the Pb^{2+} detection, different amounts of Pb^{2+} were added into 10 mM MES-Tris buffer (pH = 5.0) containing 4.0 μM DNA, 4.0 μM AMT, and the resulting solution was incubated for 5 min. The emission spectra were then recorded immediately.

1.3 Circular Dichroism.

The circular dichroism (CD) spectra were recorded using a Chirascan

circular dichroism instrument (Applied Photophysics Ltd). The wavelength range of the spectrum acquisition is 220 nm to 320 nm. The quartz cuvette cell with an optical path of 1 cm is selected. The scanning rate of the instrument is set to 100 nm/min and the response time is 2 s. The background signal was subtracted from each experimental data.

1.4 Real Sample Assay.

The human serum was prepared according to our previous report[1]. First; the human serum (2.0 mL) was mixed with ethanol (2.0 mL). After sufficient stirring, the solution was stored in a refrigerator (4℃) overnight. After the human serum/ethanol complex was centrifuged at 15000 rpm for 15 min, the supernatant was collected in an ultrafiltration centrifuge tube (Amicon Ultra-0.5 mL, Millipore) with the cut-off molecular weight of 3 kD, and was then centrifuged again at 1300 rpm for 20 min at 4℃. The filtrate was stored for further use. 4.0 μM DNA and 4.0 μM AMT and different concentrations of Pb^{2+} were added to 10 mM MES-Tris buffer (pH=5.0) containing 1% human serum.

Reference

1. Jiang. X., Geng. F., Wang. Y., Liu. J., Qu. P. and Xu. M., *Biosen. Bioelectron.*, **2016**, *81*, 268-273.

2. Optimization of experimental conditions

First, the kinetic of time-dependent fluorescent intensity of the designed sensor upon the addition of different concentrations of Pb^{2+} at 2.0 μM, 2.5

μM and 3.0 μM were recorded (Fig. S2). The fluorescence of AMT/T30695 complex is very low and the fluorescence change was ignorable in the absence of Pb^{2+} over the experiment time (30 min). As typically described in Fig. S2, the fluorescence emission intensity of AMT increases with the increasing concentrations of Pb^{2+} in the first 5 min, after which the fluorescence signal was saturated. These results suggest that the kinetics of the sensing system to Pb^{2+} were fast. Therefore, the time of 5 min was recommended as the incubation time after adding Pb^{2+} samples and then the fluorescence intensities of the sensing system were monitored in the subsequent experiments after vigorously stirring for 30 s.

In order to obtain the best sensing performance, the measurement conditions were optimized. The concentration of K^+ was optimized first because G-quadruplexes generally require monovalent cations such as K^+ to stabilize their structure. So the concentration of K^+ causes great effect to the sensing performances of the designed biosensor. Fig. S3 reveals the relative fluorescence intensity (F/F_0) is decreased with the increasing concentrations of K^+, where F and F_0 was the maximum fluorescence intensity of the developed biosensor in the presence and the absence of Pb^{2+}, respectively. The reason for the effect was initially assumed to the high stability of the formed G-quadruplexes in the presence of K^+. However, if the stability of the G-quadruplexes is too high, it is not conducive to replacing the AMT from the G-quadruplex/AMT complex. Therefore, K^+ was not included in

the work. It is well-known that pH has a great effect on the fluorescence intensity of the fluorophore. At the same time, pH also affects the existing form of Pb^{2+} in aqueous solutions. As presented in Fig. S4, an acidic pH of 5.0 was used in the following experiments. Next, the effects of the ratio of T30695 and Z were examined. The results (Fig. S5) showed the ratio of T30695 and Z of 1:3 could give the highest sensitivity. The effect of DNA concentration on sensitivity was evaluated. At a low total DNA concentration, the quenching efficiency of AMT was low. The high background signal reduces the sensitivity. The excess DNA at higher total DNA concentration could quench the displaced AMT again. Thus the sensitivity was also reduced. As shown in Fig. S6, the total DNA concentration of 3 μM was selected. Finally, it has been well-known that a lower probe concentration will help to achieve higher detection sensitivity (Yuan et al. 2013; Guo et al. 2015). Thus, 3 μM AMT was considered as an optimal concentration in this work (Fig. S7).

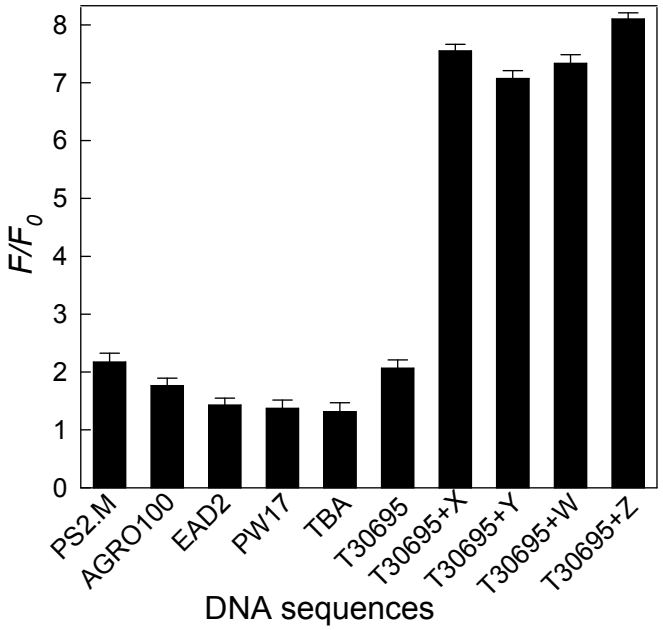

Figure S1 Comparison of fluorescent response to 5 μM Pb^{2+} in 10 mM MES-Tris buffer with different DNA sequences at the concentration of 4 μM. The concentration of AMT was fixed at 4 μM. λex= 340 nm and λex= 450 nm. All error bars are the result of three independent mesurements.

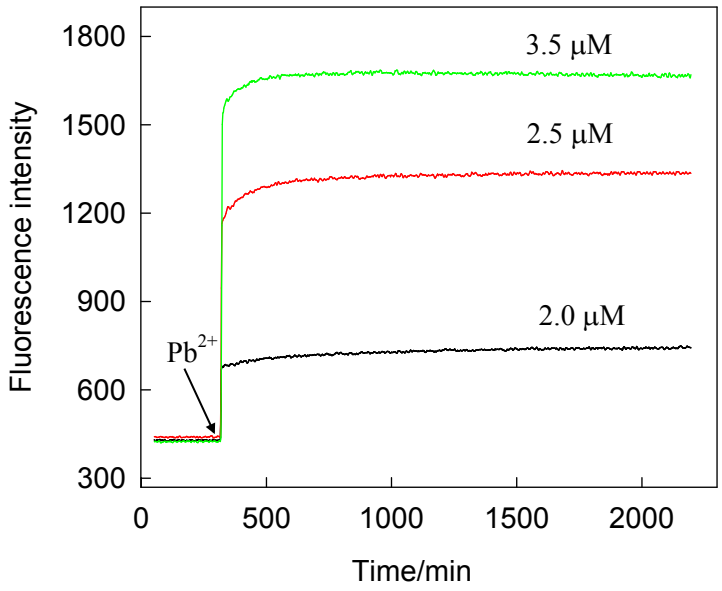

Figure S2 Time course of fluorescent increase in the presence of different concentrations of Pb^{2+} in 10 mM MES-Tris buffer (pH 5.0) containing 4 μM DNA and 4 μM AMT. λem= 450 nm and λex= 340 nm.

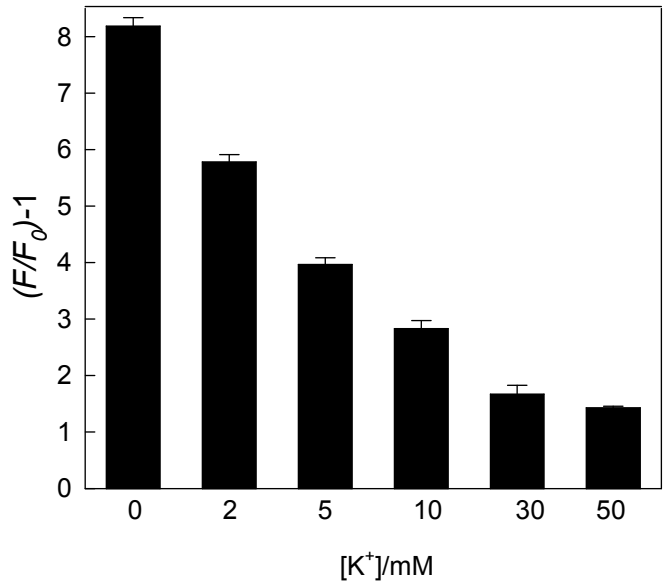

Figure S3 K^+ concentration optimization. Experiments were carried out in 10 mM MES-Tris buffer (pH 5.0) containing 4 μM DNA, 4 μM AMT and 5 μM Pb^{2+} with varying amounts of K^+. λem= 450 nm and λex= 340 nm. The error bars represent the standard deviation (n = 3).

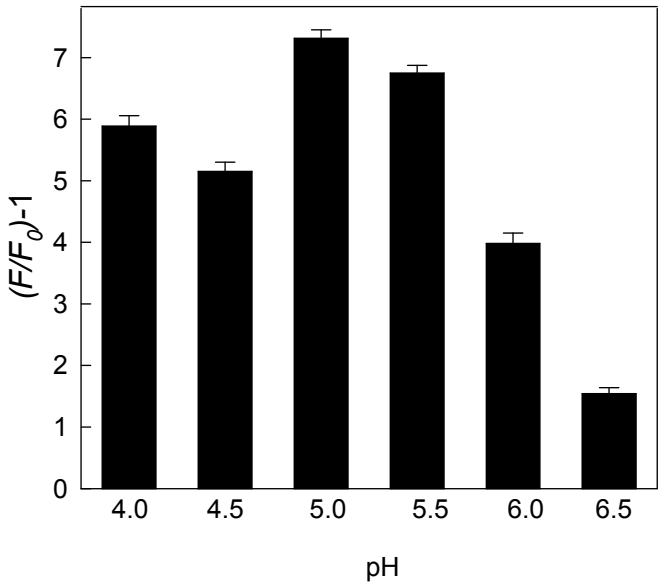

Figure S4 Effect of pH on the sensing performance. Experiments were carried out in 10 mM MES-Tris buffer (pH 5.0) containing 4 μM DNA, 4 μM AMT and 5 μM Pb^{2+} with varying pH from 4.0 to 6.5. λem= 450 nm and λex= 340 nm. The error bars represent the standard deviation (n = 3).

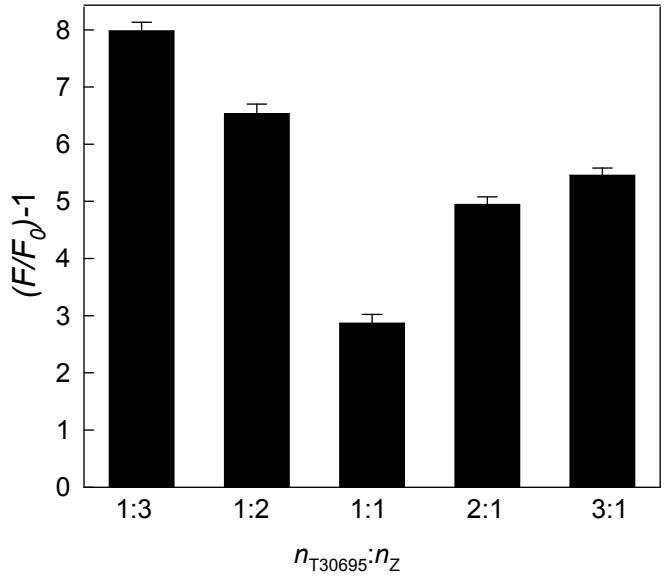

Figure S5 Effect of the molar ratio of T30695 to Z on the sensing performance. Experiments were carried out in 10 mM MES-Tris buffer (pH 5.0) containing 4 μM DNA, 4 μM AMT and 5 μM Pb^{2+} with different molar ratios of T30695 to Z. λem= 450 nm and λex= 340 nm. The error bars represent the standard deviation (n = 3).

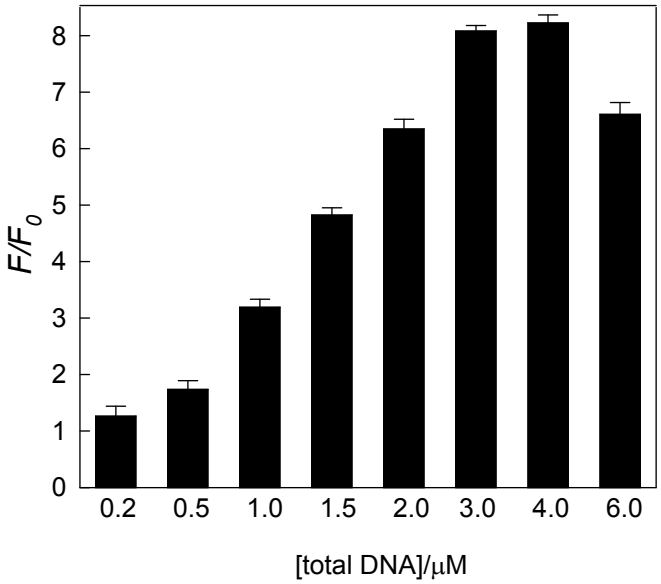

Figure S6 DNA concentration optimization. Experiments were carried out in 10 mM MES-Tris buffer (pH 5.0) containing 4 μM AMT and 5 μM Pb^{2+} with varying amounts of DNA. λem= 450 nm and λex= 340 nm. The error bars represent the standard deviation (n = 3).

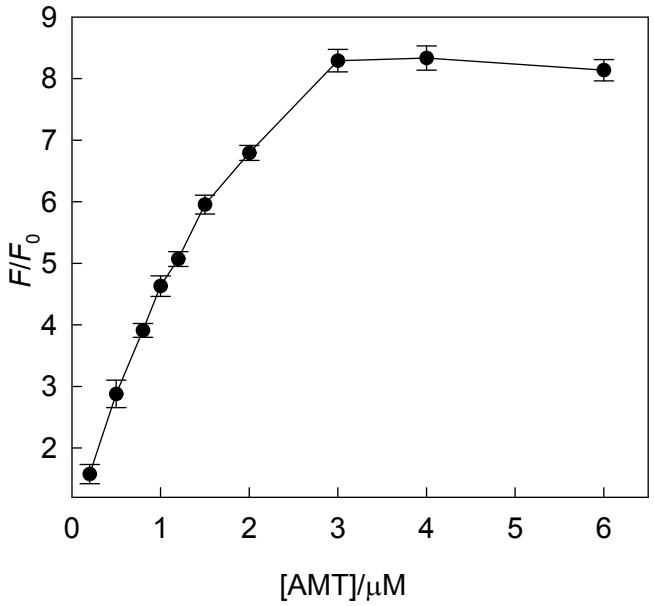

Figure S7 AMT concentration optimization. Experiments were carried out in 10 mM MES-Tris buffer (pH 5.0) containing 4 μM DNA and 5 μM Pb^{2+} with varying amounts of AMT. λem= 450 nm and λex= 340 nm. The error bars represent the standard deviation (n = 3).

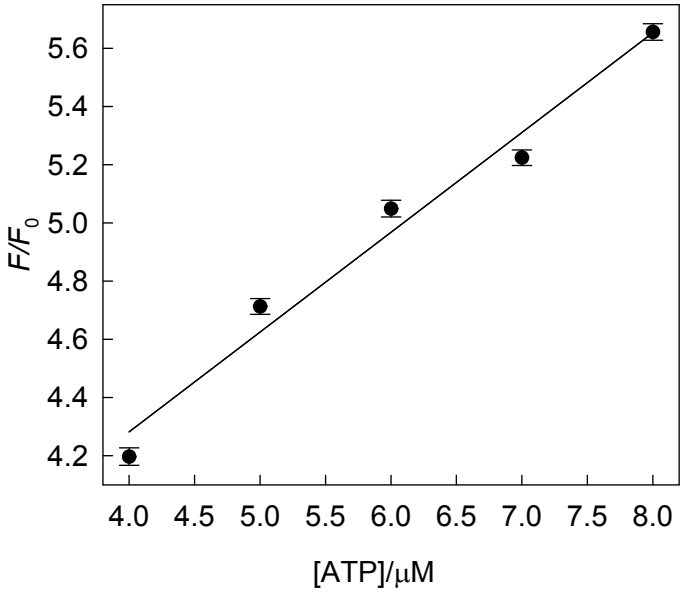

Figure S8 Working curve of high Pb^{2+} concentration obtained by addition of various concentrations of Pb^{2+} in 10 mM MES-Tris buffer (pH 5.0) containing 4 μM AMT and 4 μM DNA. The emission intensity at 450 nm is linearly proportional to the concentration of the Pb^{2+} concentration in the 4.0-8.0 μM. The linear regression equation was set as y = 0. 3429x+2.9104 (r =0.98). (y: the relative fluorescence intensity (F/F_0) at 450nm, F and F_0 were the maximum fluorescence intensity of the developed sensing system in the presence and the absence of Pb^{2+}, respectively; x, Pb^{2+} concentration)

λ ex= 340 nm. The error bars represent the standard deviation (n = 3).

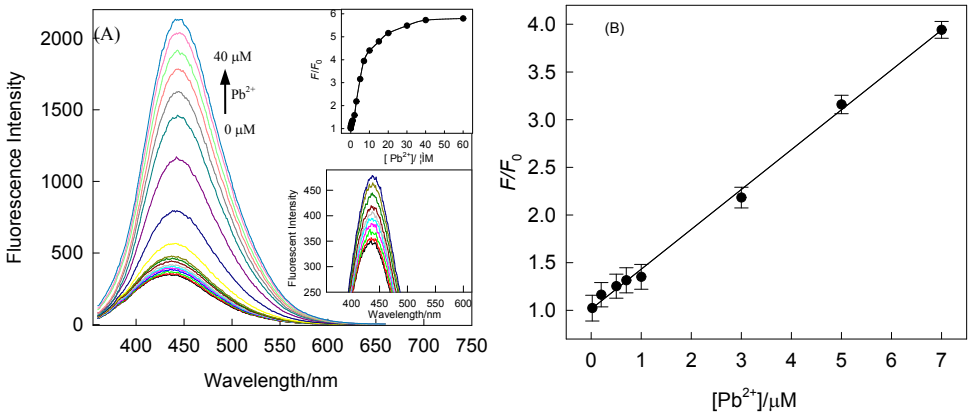

Figure S9 Fluorescent spectra of the proposed sensing system in the presence of different amount of Pb^{2+} (from 0 to 40.0 μM) in 10 mM MES-Tris (pH 5.0)buffered 1% humn serum containing, 4 μM AMT and 4 μM DNA. The inset shows the evolution of maximum fluorescent intensity vs the concentration of Pb^{2+}. λex=340 nm. (B) Linear plot of the relative fluorescence intensity (F/F_0) as a function of the increasing concentrations of Pb^{2+}. F and F_0 were the maximum fluorescence intensity of the developed sensing system in the presence and the absence of Pb^{2+}, respectively. The linear regression equation was set as y = 0. 4178x+1.0144 (r =0.998). (y: the relative fluorescence intensity (F/F_0) at 450nm,; x, Pb^{2+} concentration)

λ ex= 340 nm. The error bars represent the standard deviation (n = 3).

Table S1 DNA sequences used for this study.

Name	Sequences
PS2.M	5’-GTG GGT AGG GCG GGT TGG-3’
AGRO100	5’-GGT GGT GGT GGT TGT GGT GGT GGT GG-3’
EAD2	5’-CTG GGA GGG AGG GAG GGA-3’
PW17	5’-GGG TAG GGC GGG TTG GG-3’
TBA	5’-GGT TGG TGT GGT TGG-3’
T30695	5’-GGG TGG GTG GGT GGG T-3’ 16
X	5′-CACCCTCCCAC-3′
Y	5′-CCCACCCTCCCACCCA-3′
Z	5’-AAACCCTCCCACCCACCC-3’
W	5’-CCCACCCACCCACCCA-3’

Table S2 Summary of analytical response of the proposed sensor to the reported methods.

Technique	Dynamic range	LOD	Reference
Colorimetric	10-500 nM	25 nM	1
Ratiometric Fluorescence	0–4.0 μM	3.4 nM	2
Fluorescence		10 nM	3
UV–vis spectroscopy	0.03-2 μM	13 nM	4
Ratiometric Fluorescence		23.5 nM	5
Fluorescence		34 nM	6
Fluorescence	0-190 nM	10 nM	7
Fluorescence	25 nM -0.25 μM	3.5 nM	8
Fluorescence	0-500 nM	15 nM	9
Electrochemical	5-30 μg/L (ppb)	21 nM (4.4 ppb)	10
Fluorescence	20 nM to 1 μM	20 nM	11
This Work	0.1-1.0 μM 4.0-8.0 μM	3.6 nM	

Reference

1. Wang, D.; Ge, C.; Lv, K.; Zou, Q.; Liu, Q.; Liu, L.; Yang, Q.; Bao, S., A simple lateral flow biosensor for rapid detection of lead(ii) ions based on G-quadruplex structure-switching. *Chem. Commun.* **2018,** *54* (97), 13718-13721.
2. Zhang, D.; Zhu, M.; Zhao, L.; Zhang, J.; Wang, K.; Qi, D.; Zhou, Y.; Bian, Y.; Jiang, J., Ratiometric Fluorescent Detection of Pb^{2+} by FRET-Based Phthalocyanine-Porphyrin Dyads. *Inorganic Chemistry* **2017,** *56* (23), 14533-14539.
3. Yu, Z.; Zhou, W.; Han, J.; Li, Y.; Fan, L.; Li, X., Na^{+}-Induced Conformational Change of Pb^{2+}-Stabilized G-Quadruplex and Its Influence on Pb^{2+} Detection. *Analytical Chemistry* **2016,** *88* (19), 9375-9380.
4. Yu, Y.; Hong, Y.; Gao, P.; Nazeeruddin, M. K., Glutathione Modified Gold Nanoparticles for Sensitive Colorimetric Detection of Pb^{2+} Ions in Rainwater Polluted by Leaking Perovskite Solar Cells. *Analytical Chemistry* **2016,** *88* (24), 12316-12322.
5. Peng, D.; Li, Y.; Huang, Z.; Liang, R.-P.; Qiu, J.-D.; Liu, J., Efficient DNA-Catalyzed Porphyrin Metalation for Fluorescent Ratiometric Pb^{2+} Detection. *Analytical Chemistry* **2019,** *91* (17), 11403-11408.
6. Lu, H.; Xu, S.; Liu, J., One Pot Generation of Blue and Red Carbon Dots in One Binary Solvent System for Dual Channel Detection of Cr^{3+} and

Pb^{2+} Based on Ion Imprinted Fluorescence Polymers. *ACS Sensors* **2019,** *4* (7), 1917-1924.

7. Bain, D.; Maity, S.; Paramanik, B.; Patra, A., Core-Size Dependent Fluorescent Gold Nanoclusters and Ultrasensitive Detection of Pb^{2+} Ion. *ACS Sustainable Chemistry & Engineering* **2018,** *6* (2), 2334-2343.
8. Zhu, H.; Yu, T.; Xu, H.; Zhang, K.; Jiang, H.; Zhang, Z.; Wang, Z.; Wang, S., Fluorescent Nanohybrid of Gold Nanoclusters and Quantum Dots for Visual Determination of Lead Ions. *ACS Applied Materials & Interfaces* **2014,** *6* (23), 21461-21467.
9. Yang, C.; Yang, S.; Li, J.; Du, Y.; Song, L.; Huang, D.; Chen, J.; Zhou, Q.; Yang, Q.; Tang, Y., Intelligent Sensors of Lead Based on a Reconfigurable DNA-Supramolecule Logic Platform. *Analytical Chemistry* **2018,** *90* (17), 10585-10590.
10. Kang, W.; Pei, X.; Rusinek, C. A.; Bange, A.; Haynes, E. N.; Heineman, W. R.; Papautsky, I., Determination of Lead with a Copper-Based Electrochemical Sensor. *Analytical Chemistry* **2017,** *89* (6), 3345-3352.
11. Li, T.; Dong, S. J.; Wang, E. K., A Lead(II)-Driven DNA Molecular Device for Turn-On Fluorescence Detection of Lead(II) Ion with High Selectivity and Sensitivity, J.Am.Chem.Soc.2010, 132,13156–13157.

Table S3 Quantification of Pb^{2+} in 1% human serums using the developed sensor and ICP-AES.

Samples	Spiked Pb^{2+}/μM	Found Pb^{2+}/μM	Recovery(%)	RSD(%)	ICP-AES
1	0.2	0.30 ± 0.03	110	6.3	0.25 ± 0.02
2	0.7	0.75 ± 0.04	97	2.9	0.73 ± 0.04
3	5.0	4.81 ± 0.04	95	0.34	4.94 ± 0.08